

The continuous flow of matter that escapes out of the solar gravitational well is known as the solar wind. As the material flows out of the Sun, it is accelerated to between 400 and 800 km s⁻¹. Through this continuous flow of material, the Sun loses more than one million tonnes every second. But this is just a tiny fraction, corresponding to 2×10^{-14} of a solar mass that is lost every year. However, the solar wind does not only involve particles, it also carries the solar magnetic field lines.

The magnetized solar wind permeates the entire solar system, having an effect on any body encountered on its way. The meeting of the solar wind and a solar system planet can result in complex interactions that depend on the characteristics of both the local solar wind and the planet. Factors such as whether the planet is magnetized or whether it has an atmosphere can play different roles in this interaction.

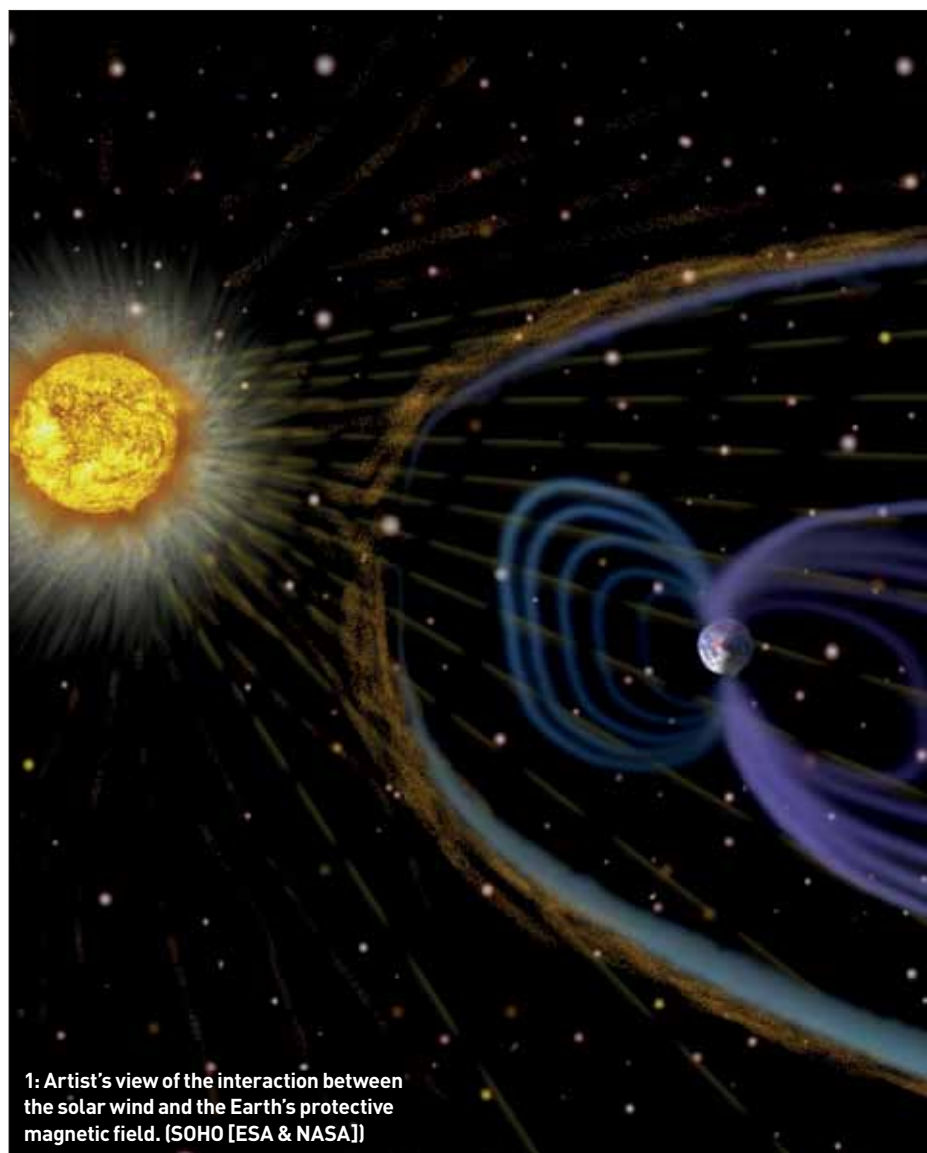
Planets that are weakly magnetized or not magnetized, such as Mars, can have their atmospheres exposed to the impact of the solar wind. The solar wind may then remove the atmosphere of the planet by sputtering processes. Evidence suggests that Mars once had a thicker atmosphere, but most of it may have disappeared due to interaction with the young Sun's wind, believed to have been more intense in the distant past.

In the case of a magnetized planet such as the Earth, the planet's field acts as a large obstacle for the solar wind: the flow of particles produced by the Sun cannot penetrate all the way to the surface of our planet, but ends up being deflected around the Earth's magnetic field lines (see figure 1). Because of the speed of the flow, the impact of the solar wind in the magnetosphere of the Earth produces a bow shock that surrounds the dayside magnetosphere of our planet (the side towards the Sun).

The formation of bow shocks is not the only signature of the interaction between the magnetized solar wind and a magnetized planet. Mediated by magnetic reconnection events, energetic electrons are released in the system. Some of these electrons spiral along planetary magnetic field lines, giving rise to cyclotron emission at radio wavelengths via a process called cyclotron maser instability. Because this kind of interaction is regulated by magnetic reconnections, it can only exist between magnetized bodies.

Exoplanetary interactions with wind

Here, three (related) processes resulting from the interaction between the solar wind and a planet were outlined, namely: the formation of a bow shock, atmospheric erosion (in non- or weakly magnetized planets) and auroral radio emission (in magnetized planets). There is no reason to doubt that similar interactions occur between the stellar wind of an exoplanet-



1: Artist's view of the interaction between the solar wind and the Earth's protective magnetic field. [SOHO [ESA & NASA]]

Protecting planets from their stars

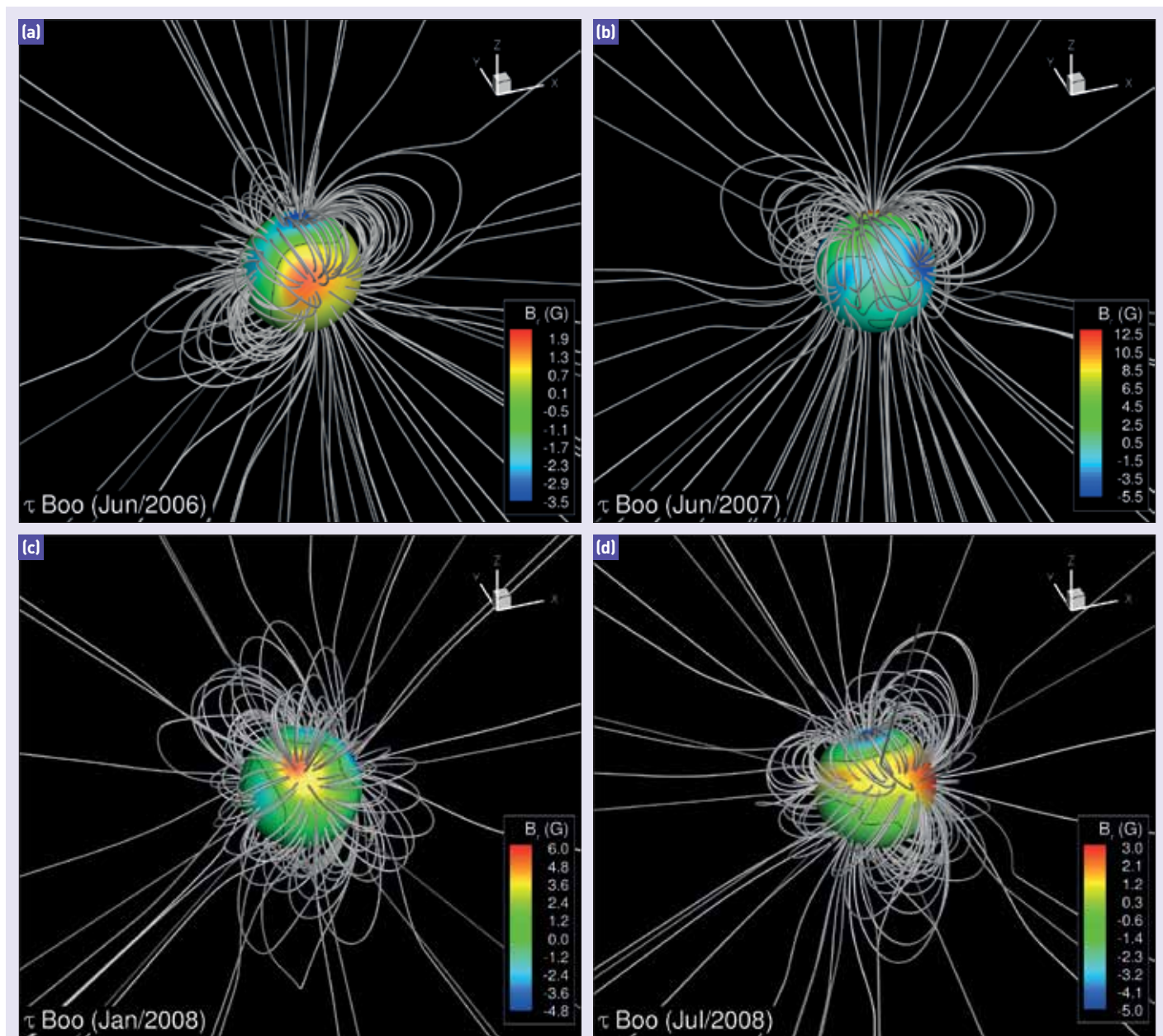
Aline Vidotto explores how planets interact with the stellar wind and how this evidence might help us find and characterize exoplanets.

hosting star and its surrounding planetary system. In fact, planetary interactions could even be more intense, as is certainly the case for stars that harbour more powerful stellar winds, or that have planets orbiting at close proximity (<0.05 au, also called close-in planets).

In the case of planetary radio emission, although the specific details of the interactions that generate these emissions are yet to be elucidated, it has been recognized that the amount of energy released at radio wavelengths by the giant planets in the solar system correlates tightly to the energy dissipated in the solar

wind-obstacle interaction (Zarka 2007). This tight linear correlation is also known as the radiometric Bode's law. Because the pressure of the solar wind is larger at smaller distances from the Sun, this correlation led scientists to propose that, if a planet were orbiting at close distance to a star identical to the Sun with the same type of stellar wind, this planet could produce radio emissions 10^3 – 10^5 times more intense than Jupiter (Zarka 2007, Jardine and Cameron 2008).

The detection of such intense auroral radio signatures from exoplanets would be a direct planet-detection method, as opposed to the



2: The lowest energy state of the coronal magnetic field of τ Boo as seen at different observing epochs. Colours denote the surface radial magnetic field and the solid line represents the neutral line (when the stellar magnetic field changes polarity).

widely used indirect methods of radial velocity measurements or transit events. Moreover, the detection of exoplanetary radio emission would also demonstrate that the planet has a magnetic field.

However, despite many attempts, exoplanetary radio emission has not yet been detected. One of the reasons for the lack of success is thought to be the beamed nature of the electron–cyclotron maser instability. Because the emission occurs over a small solid angle, it would have to be directed towards the Earth to be detected. Poor instrumental sensitivity would also explain the lack of detection of radio emission from exoplanets. Another reason for the failure to find exoplanets this way may be because of a frequency mismatch: the emission process is thought to occur at cyclotron frequencies, which depend on the intensity of the plan-

etary magnetic field. Therefore, planets with magnetic field strengths of a few G, for example, would emit at a frequency that could not be observed from the ground either due to the Earth’s ionospheric cut-off, or because it does not correspond to the operating frequencies of available instruments. In that regard, the low-operating frequency of LOFAR (currently under commission), jointly with its high sensitivity at this low-frequency range, makes it an instrument that has great potential to detect radio emission from exoplanets.

Note that different properties of star–planet systems can also give rise to physical interactions that are absent or negligible in the solar system. For instance, it has been suggested that the winds of young Sun-like stars could change the orbital angular momentum of planets by the action of dragging forces, causing planetary

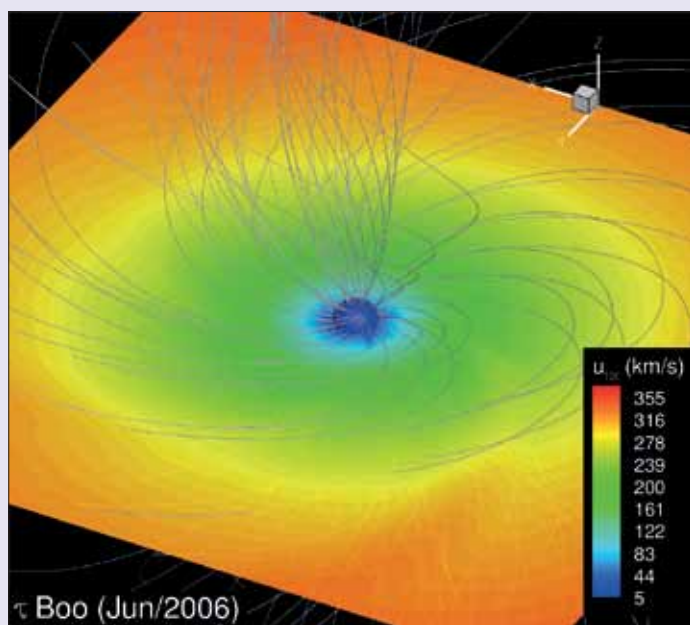
migration (Lovelace *et al.* 2008). In the solar system, this process is negligible, but could be important in particular circumstances of stars that harbour strong magnetic fields and dense winds (Vidotto *et al.* 2009, 2010b) or for synchronizing stellar rotation with the orbital motion of planets during the pre-main-sequence phase (Lanza 2010).

Independently of the process involved, it is worth noting that, in order to study the interaction of the planets with the local environment in which they are immersed, a key step is to understand the magnetic coronae and winds of the host stars.

Stellar magnetic fields

Although we seem to comprehend reasonably well the properties of the solar wind (especially because we are immersed in it), it is much more

3: Final configuration of the steady-state magnetic field of τ Boo for June 2006. Colours denote the stellar wind velocity on the equatorial plane (xy plane). Stellar rotation axis is along positive z.



difficult to probe and identify the properties of the winds of other stars. Even if we concentrate on a subsample of stars with similar masses to our Sun, differences in coronal temperatures, stellar rotation rates, magnetic field intensities, etc, imply different stellar wind properties. Because of that, theoretical and numerical models are essential in the progress of our understanding of winds of other stars.

One factor of particular relevance for stellar winds is the geometry of the stellar magnetic field. The Sun can again be a useful illustration. During periods of minimum activity, the solar field topology resembles an aligned dipole. The fast solar wind emerges from the polar regions where magnetic field lines are open (coronal holes) and the slow solar wind emerges above the low-latitude active regions (latitudes of up to $30\text{--}35^\circ$ around the equator). In contrast, during periods of maximum activity, the topology of the field becomes more complicated, affecting the solar wind: by the time the Sun is at maximum activity, the poles also emit the slow solar wind.

Although the richness of details of the magnetic field configuration is only known for our closest star, modern techniques have made it possible to reconstruct the large-scale surface magnetic fields of other stars. The Zeeman–Doppler Imaging (ZDI) technique is a tomographic imaging technique (e.g. Donati and Brown 1997) that allows the reconstruction of the large-scale magnetic field (intensity and orientation) at the surface of the star from a series of circular polarization spectra. This method has now been used to investigate the magnetic topology of planet-hosting stars (Fares *et al.* 2009, 2010, 2012), solar-type stars (Petit *et al.* 2008, 2009), young solar-type stars (Marsden *et al.* 2006; Donati *et al.* 2008b, 2010; Husain *et al.* 2007), low-mass stars (Donati *et al.*

2006a, 2008a; Morin *et al.* 2008, 2010) and high-mass stars (Donati *et al.* 2006b). Donati and Landstreet (2009) present a recent overview of the survey.

Although some objects host fields that can resemble the large-scale solar field, there are also fascinating differences. For example, solar-type stars that rotate about twice as fast as our Sun show a substantial toroidal component of magnetic field, a component that is almost non-existent in the large-scale surface solar magnetic field (Petit *et al.* 2008). The magnetic topology of low-mass ($<0.5 M_\odot$) very active stars seem to be dictated by interior structure changes: while partly convective stars possess a weak non-axisymmetric field with a significant toroidal component, fully convective ones exhibit strong poloidal axisymmetric dipole-like topologies (Morin *et al.* 2008, Donati *et al.* 2008a).

All this recent insight into the magnetic topology of different stars can now be incorporated in stellar wind models, which is a key step to make them more realistic. Ultimately, it is the characterization of the stellar wind that will constrain the local environment surrounding exoplanets and, consequently, their interactions with the host-star plasma.

The τ Boo system

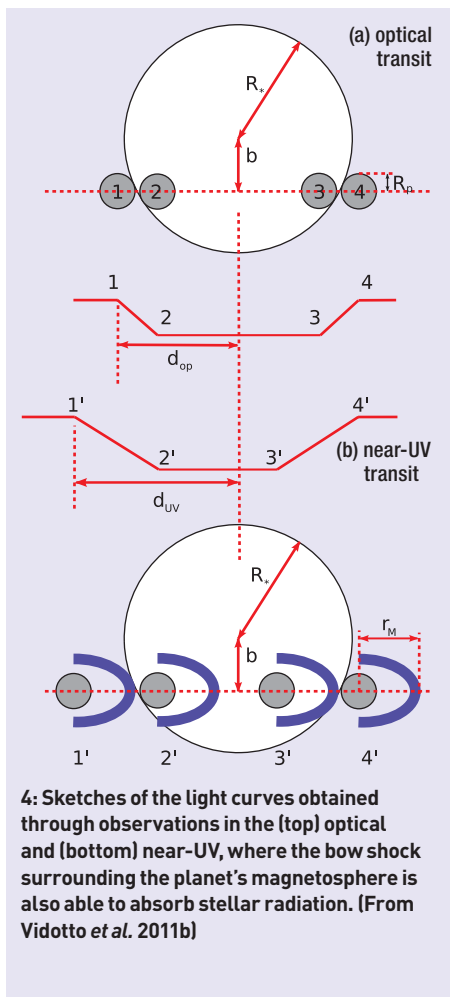
A particular exoplanetary system that has been placed under scrutiny is the τ Boo system. The host-star, τ Boo (spectral type F7V), is a remarkable object, not only because it hosts a giant planet orbiting very close to it (0.046 au), but also because it is the only star other than the Sun for which a full magnetic cycle has been reported in the literature. So far, two polarity reversals have been detected (Donati *et al.* 2008c, Fares *et al.* 2009), suggesting that the star undergoes magnetic cycles similar to the Sun, but with a complete period that is about

one order of magnitude smaller (about 2 years as opposed to 22 years for the solar magnetic cycle). The polarity reversals in τ Boo seem to occur roughly every year, switching from a negative poloidal field near the visible pole in June 2006 (the intensity of the surface field is colour-coded in figure 2a) to a positive poloidal field in June 2007 (figure 2b), and then back again to a negative polarity in July 2008 (figure 2d; Catala *et al.* 2007, Donati *et al.* 2008c, Fares *et al.* 2009).

The nature of such a short magnetic cycle in τ Boo remains an open question. Surface differential rotation is thought to play an important role in the solar cycle. The fact that τ Boo presents a much higher level of surface differential rotation than that of the Sun may be responsible for its short observed cycle. In addition, τ Boo hosts a close-in planet that, due to its proximity to the star, may have been able to synchronize, through tidal interactions, the rotation of the shallow convective envelope of the host F-type star with the planetary orbital motion. This presumed synchronization may have enhanced the shear at the tachocline, which may have influenced the magnetic cycle of the star (Fares *et al.* 2009).

Because the stellar winds of cool stars are magnetic by nature, variations of the stellar magnetic field during the cycle directly influence the outflowing wind. Therefore, the rapid variation of the large-scale magnetic field of τ Boo implies that the environment surrounding the close-in planet should be varying quite rapidly too. In order to characterize such an environment and the related interactions with the exoplanet, Vidotto *et al.* 2012 performed three-dimensional magnetohydrodynamics simulations of the host star's wind, taking into account the observed surface magnetic maps of τ Boo.

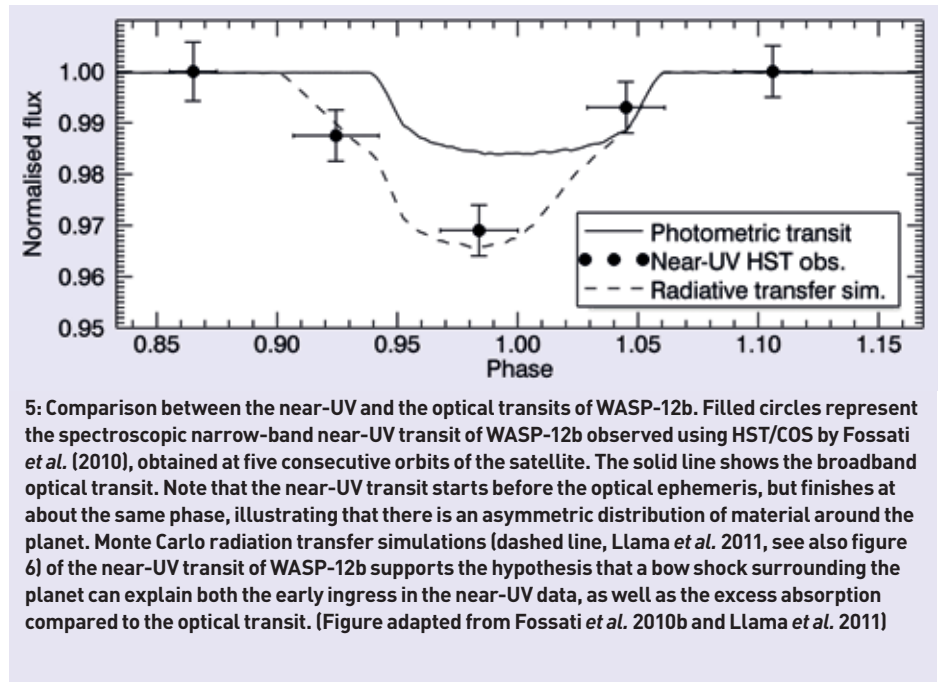
To incorporate these surface maps in the simulations, one needs a way to extrapolate the surface magnetic field to the stellar corona. A common method for doing this is by using the assumption that the magnetic field is at its lowest energy state (Altschuler and Newkirk 1969, Jardine *et al.* 1999). Figure 2 shows the derived extrapolated coronal magnetic field lines for each of the observed epochs for which surface maps have been observationally reconstructed. The lowest-energy magnetic field configuration (the potential field) is used in simulations of stellar winds as an initial condition only. In fact, the interaction between the stellar wind particles and the magnetic field lines removes the coronal field from its lowest energy state. This is illustrated in figure 3, which shows the final steady-state configuration of the magnetic field lines of τ Boo at the observed epoch of June 2006. The stress in the magnetic field lines is verified by the presence of twisted magnetic field lines around the rotation axis (z-axis). Figure 3 shows



the wind velocity in the equatorial plane of the star (xy -plane). Vidotto *et al.* (2012) showed that both the coronal magnetic field lines and the stellar wind velocity profile vary through the stellar cycle.

One important unknown parameter that is needed in all models of stellar winds is the density at the base of the corona. Unfortunately, without a good estimate of this value, the stellar mass-loss rates, one of the fundamental properties of the stellar wind, cannot be inferred. One way to constrain coronal base densities, and therefore mass-loss rates, is to perform a direct comparison between derived mass-loss rates from the simulations and those determined observationally. However, mass-loss rate measurements exist only for the Sun, so indirect approaches are often employed (see, for example, Wood 2004).

Vidotto *et al.* 2012 employed an indirect methodology to constrain the mass-loss rate of τ Boo using emission measure (EM) values derived from X-ray spectra. The EM probes both the electron and ion densities inside regions of closed magnetic field lines in the stellar corona. Therefore, by tuning the coronal densities in the simulation, it is possible to find a best match of the predicted EM values from the simulations to the observed ones for τ Boo. This approach constrained the mass-loss rate \dot{M}



of τ Boo, showing that this star probably has a denser wind than that of the Sun, with mass-loss rates that are two orders of magnitude larger than the solar value \dot{M}_\odot ($\dot{M} \approx 135 \dot{M}_\odot$).

Planetary radio emission in τ Boob

Such a denser wind implies that the energy dissipated in the stellar wind–planet interaction can be significantly higher than the values derived in the solar system. Since, among the solar system planets, the wind-dissipated energy follows linearly the planetary radio emission, it is expected that the planet τ Boob should have high radio emission, provided that the planet is magnetized and the proper viewing conditions are achieved. Combined with the close proximity of the system (~ 16 pc), the τ Boob system is one of the strongest candidates for verifying planetary radio emission theories.

Using the detailed stellar wind model developed for its host-star, Vidotto *et al.* (2012) estimated radio emission from τ Boob, exploring different values for the assumed planetary magnetic field. They showed that, for a planet with a magnetic field similar to Jupiter's (≈ 14 G), the radio flux is estimated to be ≈ 0.5 – 1 mJy, occurring at an emission frequency of ≈ 34 MHz. Although small, this emission frequency lies in the observable range of current instruments, such as LOFAR. To observe such a small flux, an instrument with a sensitivity lying on a mJy level is required.

The same estimate was made considering that the planet has a magnetic field similar to the Earth (≈ 1 G). Although the radio flux is not significantly different to the previous case, the emission frequency (≈ 2 MHz) falls at a range below the ionospheric cut-off, preventing any possible detection from the ground. In fact, because of the ionospheric cutoff at ~ 10 MHz,

radio detection with ground-based observations from planets with magnetic field intensities $\lesssim 4$ G should not be possible (Vidotto *et al.* 2012).

Finding magnetized planets

A magnetic field has not yet been observed on extrasolar planets. Detection of radio emission would not only constrain local characteristics of the stellar wind, but would also demonstrate that exoplanets are magnetized. Fortunately, there may be other ways to probe exoplanetary magnetic fields, in particular for transiting systems, through signatures of bow shocks during transit observations.

The formation of bow shocks is one signature of the interaction of the host-star corona/wind with an orbiting planet. What determines the orientation of the shock is the net velocity of the particles meeting the planet's magnetosphere. In the case of the Earth, the solar wind has essentially only a radial component, which is much larger than the orbital velocity of the Earth. Because of that, the shock forms facing the Sun (a dayside shock). However, for close-in exoplanets that possess high orbital velocities and are frequently in regions where the host star's wind velocity is comparatively much smaller, a shock may develop ahead of the planet (called the ahead shock). In general, we expect that shocks are formed at intermediate angles.

Due to their high orbital velocities, close-in planets offer the best conditions for transit observations of bow shocks. If the compressed shocked material is able to absorb stellar radiation, then the signature of bow shocks may be observed through both a deeper transit and an early ingress of some spectral lines with respect to the broadband optical ingress (Vidotto *et al.* 2012). The sketches shown in figure 4 illustrate this idea.



6: Sequence of images from Monte Carlo radiation transfer simulations of the near-UV transit of WASP-12b. (Adapted from Llama *et al.* 2011)

This suggestion proposed by Vidotto (2010a) was motivated by transit observations of the close-in giant planet WASP-12b. Based on Hubble Space Telescope/Cosmic Origins Spectrograph (HST/COS) observations using narrow-band near-UV spectroscopy, Fossati *et al.* (2010b) showed that the transit lightcurve of WASP-12b (filled circles in figure 5) presents both an early ingress when compared to its optical transit (solid line in figure 5), as well as excess absorption during the transit, indicating the presence of an asymmetric distribution of material surrounding the planet. This result was reiterated by Haswell *et al.* (2012) in a more recent HST/COS set of observations.

WASP-12b orbits a late-F main-sequence star which has mass $M_* = 1.35M_\odot$ and radius $R_* = 1.57R_\odot$, at an extremely small orbital radius of $a = 0.023$ au, which corresponds to a distance of only $3.15R_*$ (Hebb *et al.* 2009). Due to its close proximity to the star, the flux of coronal particles impacting on the planet should come mainly from the azimuthal direction, as the planet moves at a Keplerian orbital velocity of $u_K = (GM_*/a)^{1/2} \sim 230 \text{ km s}^{-1}$ around the star. Therefore, stellar coronal material is compressed ahead of the planetary orbital motion, possibly forming a bow shock ahead of the planet. Vidotto *et al.* (2010a) suggest that this shocked material is able to absorb enough stellar radiation, causing the asymmetric lightcurve observed in the near-UV (see figures 4 and 5), where the presence of compressed material ahead of the planetary orbit causes the early ingress, while the lack of compressed material behind the planetary orbit causes simultaneous egresses both in the near-UV transit and the optical one.

To verify this idea, Llama *et al.* (2011) performed Monte Carlo radiation transfer simulations of the near-UV transit of WASP-12b. They confirmed that the presence of a bow shock indeed breaks the symmetry of the transit lightcurve, supporting the hypothesis proposed by Vidotto *et al.* (2010a). In their simulations, the geometry of the shock was varied in order to fit the near-UV data. They found that no fine-tuning is required. There are several shock geometries that could still provide a good fit to the HST/COS data; the current data is not yet adequate to fully constrain the bow shock geometry. The dashed line in figure 5 shows one of the several possible fits found by Llama *et*

al. (2011). Figure 6 shows a sequence of images depicting the transit in the near-UV, where we note that the shocked material can be very tenuous, but as long as there is enough material integrated along the line of sight, it can cause the absorption level observed in the near-UV data.

Planetary magnetic fields: a new detection method?

An interesting outcome of the observations of bow shocks around exoplanets is that it permits one to infer the magnetic field intensity of the transiting planet. By measuring the phases at which the near-UV and the optical transits begin, one can derive the stand-off distance from the shock to the centre of the planet. In the geometrical consideration below, we assume that the planet is fully superimposed on the disc of the central star, which is a good approximation for the cases of, for example, small planets and transits with small impact parameters b . Consider the sketches presented in figure 4, where d_{op} and d_{uv} are, respectively, the sky-projected distances that the planet (optical) and the system planet+magnetosphere (near-UV) travel from the beginning of the transit until the middle of the optical transit

$$d_{op} = (R_*^2 - b^2)^{1/2} + R_p \quad (1)$$

and

$$d_{uv} = (R_*^2 - b^2)^{1/2} + r_M \quad (2)$$

where b is the impact parameter derived from transit observations, R_p is the planetary radius, and r_M is the distance from the shock nose to the centre of the planet. The start of the optical transit occurs at phase $\phi_1 \equiv \phi_{op}$ (point 1 in figure 4a), while the near-UV transit starts at an earlier phase $\phi_1' \equiv \phi_{uv}$ (point 1' in figure 4b). Taking the optical mid-transit phase at $\phi = \phi_m \equiv 1$, we note that d_{op} is proportional to $(1 - \phi_{op})$, while d_{uv} is proportional to $(1 - \phi_{uv})$. Using equations 1 and 2 we find (Vidotto *et al.* 2010a, 2011d)

$$\frac{r_M}{R_p} = \frac{(1 - \phi_{uv})}{(1 - \phi_{op})} \left[\sqrt{\left(\frac{R_*}{R_p}\right)^2 - \left(\frac{bR_*}{R_p}\right)^2} + 1 \right] - \sqrt{\left(\frac{R_*}{R_p}\right)^2 - \left(\frac{bR_*}{R_p}\right)^2} \quad (3)$$

Note that, by measuring the phase at which the transit starts in the near-UV (ϕ_{uv}), one can relate the normalized stand-off distance (r_M/R_p) to observed quantities such as the planet-star radius ratio (R_p/R_*), the impact parameter (b , in units of R_*), and the phase of optical first contact (ϕ_{op}).

We assume the stand-off distance to trace the extent of the planetary magnetosphere. At the magnetopause, pressure balance between the coronal total pressure and the planet total pressure requires that

$$\rho_c \Delta u^2 + \frac{[B_c(a)]^2}{8\pi} + p_c = \frac{[B_p(r_M)]^2}{8\pi} + p_p \quad (4)$$

where ρ_c , p_c and $B_c(a)$ are the local coronal mass density, thermal pressure, and magnetic field intensity, and p_p and $B_p(r_M)$ are the planet thermal pressure and magnetic field intensity at r_M . In the case of a magnetized planet with a magnetosphere of a few planetary radii, the planet total pressure is usually dominated by the contribution from the planetary magnetic pressure (i.e. $p_p \sim 0$).

Vidotto *et al.* (2010a) showed that, because WASP-12b is close to the star, the kinetic term of the coronal plasma may be neglected in equation 4. They also neglected the coronal thermal pressure (justified by the low coronal densities), so that equation 4 reduces to $B_c(a) \simeq B_p(r_M)$. Further assuming that stellar and planetary magnetic fields are dipolar, we have

$$B_p = B_* \left(\frac{R_*/a}{R_p/r_M} \right)^3 \quad (5)$$

where B_* and B_p are the magnetic field intensities at the stellar and planetary surfaces, respectively. Here as well, the planetary magnetic field can be related to observed quantities.

Therefore, by determining the phase at which the near-UV transit begins, one can derive the stand-off distance (equation 3) and then estimate the intensity of the magnetic field of the planet (equation 5), provided that the stellar magnetic field is known. For WASP-12, we use the upper limit of $B_* < 10$ G (Fossati *et al.* 2010a) and the stand-off distance obtained from the near-UV transit observation $r_M = 4.2 R_p$ (Lai *et al.* 2010) and we were able to predict an upper limit for WASP-12b's planetary magnetic field of $B_p < 24$ G.

Searching for magnetic fields in other exoplanets

In theory, the suggestion that through transit observations one can probe the planetary magnetic field is quite straightforward – all it requires is a measurement of the transit ingress phase in the near-UV. In practice, however, acquisition of near-UV transit data requires the

use of space-borne facilities, making follow-up and new target detections rather difficult.

In order to optimize target selection, Vidotto *et al.* (2011a) presented a classification of the known transiting systems according to their potential for producing shocks that could cause observable light curve asymmetries. The main assumption considered was that, once the conditions for shock formation are met, planetary shocks absorb in certain near-UV lines, in a similar way to WASP-12b. In addition, for it to be detected, the shock must compress the local plasma to a density sufficiently high to cause an observable increase in optical depth.

This last hypothesis requires knowledge of the local ambient medium that surrounds the planet.

By adopting simplified hypotheses, namely that up to the planetary orbit the stellar corona can be treated as in hydrostatic equilibrium and isothermal, Vidotto *et al.* (2011a) predicted the characteristics of the ambient medium that surrounds the planet for a sample of 125 transiting systems, and discussed whether such characteristics present favourable conditions for the presence and detection of a bow shock. Excluding systems that are quite far ($\gtrsim 400$ pc), the planets that were top ranked are: WASP-19b, WASP-4b, WASP-18b, CoRoT-7b, HAT-P-7b, CoRoT-1b, TrES-3 and WASP-5b.

Concluding remarks

In this article, I discussed how the stellar corona/wind can affect surrounding planets. Because the winds of cool stars are incredibly tenuous, up to now there have not been any direct measurements of their properties (except for the Sun itself). To determine the fundamental properties of such winds (such as mass-loss rates, terminal velocities), one has to rely on the very few indirect methods that probe cool stellar winds. On the theoretical front, magnetohydrodynamics numerical simulations can definitely help ascertain the aspects of winds. Aiming at characterizing such winds more realistically, we have implemented (for example, Vidotto *et al.* 2011c, 2012) in our numerical simulations observationally derived surface magnetic field maps, which show the diverse magnetic field strengths and topologies that these stars host.

Ultimately, quantifying and understanding winds of cool stars leads to the characterization of the environment surrounding exoplanets. Although these environments may be potentially dangerous for a planet's atmosphere (especially for close-in planets), the interaction between planets and the host star's coronal winds can provide other avenues for planet detection (such as radio emission) and maybe even assessment of planetary properties (such as

the planet's magnetic field through bow shock observations), which would otherwise remain unknown.

Stellar wind–planet interactions are two-way roads. On one side, the stellar wind plays a decisive role in the characterization of the magnetic environment around the planet. On the other, planetary observations of wind-related processes (transit asymmetries, planetary radio emission) can help constrain the local properties of the stellar wind.

Recent observations of transiting systems reveal that transit asymmetries are common and occur at various wavelengths.

“How do different stellar coronal environments around planets affect habitability?”

Transit asymmetries are believed to be caused by an asymmetric distribution of material surrounding the planet. Rappaport (2012) reported a transit asymmetry in KIC 12557548, which they have interpreted as being caused by a trailing dust cloud. Further data on the system found variations in the transit asymmetry, leading Brogi *et al.* (2012)

to conclude that the dust cloud might have disappeared. Temporal variations of transit asymmetries were also observed in the brighter system HD 189733 (Lecavelier des Etangs *et al.* 2012). The observed variation was attributed to modifications of the properties of the stellar wind impacting on the planet, probably caused by a stellar flare detected ~ 8 h prior to the transit.

It is interesting to note that, in the framework of near-UV transit, Vidotto *et al.* (2011b) investigated time-dependent effects on the asymmetry of planetary transit light curves. For example, stellar coronae are not axisymmetric. Thus, along its orbit, the planet interacts with stellar material of different characteristics. In this case, differences in the surrounding material will cause variation in the size of the planet's magnetosphere, and therefore on the stand-off distance observed during transit observations. Because the stellar rotation period in general differs from the orbital period, a series of transit observations can probe different stellar material. This is the case, for instance, if the star has an oblique magnetosphere and the planetary orbit takes the planet through regions of confined and expanding stellar material.

Furthermore, time-dependent intrinsic variations of the stellar magnetism, such as those due to coronal mass ejections (CMEs), flares and stellar magnetic cycles, can also impress variable observable signatures in different transits of the same system. Although the impact of a CME on a planet increases the local density surrounding the planet, its effect is transient and may not be captured in transit observations, except maybe for the case of planets orbiting young, magnetically active stars for which the magnitude and

frequency of flares and CMEs may be much higher than for the present-day Sun.

We live in exciting times for both theoretical and observational investigations of the interaction between host stars and their exoplanets. Several aspects remain unsolved, such as how different stellar coronal environments surrounding a planet can affect habitability (Vidotto *et al.* 2013 submitted). The findings reviewed here highlight the importance of understanding and characterizing the magnetic environment of exoplanets, and provide guidance for future work. ●

Aline Vidotto is an RAS Research Fellow, SUPA, School of Physics and Astronomy, University of St Andrews, UK.

References

- Altschuler M D and Newkirk G 1969 *Solar Phys.* **9** 131.
- Brogi M *et al.* 2012 *Astron. & Astrophys.* **545** L5.
- Catala C *et al.* 2007 *Mon. Not. Roy. Ast. Soc.* **374** L42.
- Donati J-F and Brown S F 1997 *Astron. & Astrophys.* **326** 1135.
- Donati J-F and Landstreet J D 2009 *Ann. Rev. Astron. and Astrophys.* **47** 333.
- Donati J-F *et al.* 2006a *Science* **311** 633.
- Donati J-F *et al.* 2006b *Mon. Not. Roy. Ast. Soc.* **370** 629.
- Donati J-F *et al.* 2008a *Mon. Not. Roy. Ast. Soc.* **390** 545.
- Donati J-F *et al.* 2008b *Mon. Not. Roy. Ast. Soc.* **386** 1234.
- Donati J-F *et al.* 2008c *Mon. Not. Roy. Ast. Soc.* **385** 1179.
- Donati J-F *et al.* 2010 *Mon. Not. Roy. Ast. Soc.* **409** 1347.
- Fares R *et al.* 2009 *Mon. Not. Roy. Ast. Soc.* **398** 1383.
- Fares R *et al.* 2010 *Mon. Not. Roy. Ast. Soc.* **406** 409.
- Fares R *et al.* 2012 *Mon. Not. Roy. Ast. Soc.* **423** 1006.
- Fossati L *et al.* 2010a *Ap. J.* **720** 872.
- Fossati L *et al.* 2010b *Ap. J. Lett.* **714** L222.
- Haswell C A *et al.* 2012 *Ap. J.* **760** 79.
- Hebb L *et al.* 2009 *Ap. J.* **693** 1920.
- Hussain G A J *et al.* 2007 *Mon. Not. Roy. Ast. Soc.* **377** 1488.
- Jardine M and Cameron A C 2008 *Astron. & Astrophys.* **490** 843.
- Jardine M *et al.* 1999 *Mon. Not. Roy. Ast. Soc.* **305** L35.
- Lai D *et al.* 2010 *Ap. J.* **721** 923.
- Lanza L 2010 *Astron. & Astrophys.* **512** A77.
- Lecavelier des Etangs A *et al.* 2012 *Astron. & Astrophys.* **543** L4.
- Llama J *et al.* 2011 *Mon. Not. Roy. Ast. Soc.* **416** L41.
- Lovelace R V E *et al.* 2008 *Mon. Not. Roy. Ast. Soc.* **389** 1233.
- Marsden S C *et al.* 2006 *Mon. Not. Roy. Ast. Soc.* **370** 468.
- Morin J *et al.* 2008 *Mon. Not. Roy. Ast. Soc.* **390** 567.
- Morin J *et al.* 2010 *Mon. Not. Roy. Ast. Soc.* **407** 2269.
- Petit P *et al.* 2008 *Mon. Not. Roy. Ast. Soc.* **388** 80.
- Petit P *et al.* 2009 *Astron. & Astrophys.* **508** L9.
- Rappaport S *et al.* 2012 *Ap. J.* **752** 1.
- Vidotto A A *et al.* 2009 *Ap. J.* **703** 1734.
- Vidotto A A *et al.* 2010a *Ap. J.* **722** L168.
- Vidotto A A *et al.* 2010b *Ap. J.* **720** 1262.
- Vidotto A A *et al.* 2011a *Mon. Not. Roy. Ast. Soc.* **411** L46.
- Vidotto A A *et al.* 2011b *Mon. Not. Roy. Ast. Soc.* **414** 1573.
- Vidotto A A *et al.* 2011c *Mon. Not. Roy. Ast. Soc.* **412** 351.
- Vidotto A A *et al.* 2011d *Ast. Nachrichten* **332** 1055.
- Vidotto A A *et al.* 2012 *Mon. Not. Roy. Ast. Soc.* **423** 3285.
- Vidotto A A *et al.* 2013 *Mon. Not. Roy. Ast. Soc. submitted.*
- Wood B E 2004 *Living Reviews in Solar Physics* **1** 2.
- Zarka P 2007 *Planet. and Space Sci.* **55** 598.